HHS Public Access

Author manuscript

J Bone Miner Res. Author manuscript; available in PMC 2015 May 27.

Published in final edited form as:

J Bone Miner Res. 2005 September ; 20(9): 1548–1561. doi:10.1359/JBMR.050411.

Effects of Salmon Calcitonin on Trabecular Microarchitecture as Determined by Magnetic Resonance Imaging: Results From the QUEST Study*

Charles H Chesnut III[1], **Sharmilla Majumdar**[2], **David C Newitt**[2], **Andrew Shields**[1], **Jan Van Pelt**[1], **Ellen Laschansky**[1], **Moise Azria**[3], **Audrey Kriegman**[4], **Melvin Olson**[3], **Erik F Eriksen**[3], and **Linda Mindeholm**[3]

[1]Osteoporosis Research Group, Department of Radiology (UWMC-ORG), University of Washington Medical Center, Seattle, Washington, USA [2]Magnetic Resonance Science Center, Department of Radiology, University of California at San Francisco, San Francisco, California, USA [3]Novartis Pharmaceuticals, Basle, Switzerland [4]Novartis Pharmaceuticals, East Hanover, New Jersey, USA.

Abstract

The unique noninvasive MRI technique was used to assess trabecular microarchitecture at multiple skeletal sites in 91 postmenopausal osteoporotic women receiving nasal spray salmon calcitonin (CT-NS) or placebo over 2 years. In the distal radius and lower trochanter of the hip, individuals treated with CT-NS exhibited significant preservation of trabecular bone microarchitecture compared with placebo, where significant deterioration was shown. MRI analyses of os calcis or μCT/histomorphometric analyses of bone biopsies did not reveal consistent differences in architecture between CT-NS and placebo.

Introduction—It is postulated that the reduction in osteoporotic fracture risk in response to certain antiresorptive osteoporosis therapies is caused less by effects on bone quantity than on bone quality (specifically trabecular microarchitecture). To test this hypothesis, the QUEST study was conducted to assess the effects of nasal spray salmon calcitonin (CT-NS) or placebo on parameters of trabecular microarchitecture at multiple skeletal sites using noninvasive MRI technology and iliac crest bone biopsies by μCT/histomorphometry.

Materials and Methods—Ninety-one postmenopausal osteoporotic women were followed for 2 years (n = 46 for CT-NS, n = 45 for placebo); all women received 500 mg calcium daily. MRI measurements at distal radius, hip (T2 relaxation time [T2*]), and os calcis (obtained yearly), iliac crest bone biopsies with 2D histomorphometry and 3D μCT (obtained at study onset and conclusion), DXA-BMD at spine/hip/wrist/os calcis (obtained yearly), and markers of bone

*These data were presented in part at the 25th American Society of Bone and Mineral Research meeting, Minneapolis, Minnesota, September 19–23, 2003.

Address reprint requests to: Charles H Chesnut III, MD Osteoporosis Research Group University of Washington Medical Center 1107 NE 45th Street, Suite 440 Seattle, WA 98105-4631, USA chesnut@u.washington.edu.

Dr Chesnut serves as a consultant for Novartis. Drs Olson, Mindeholm, Eriksen, Kriegman, and Azria are employees of and own stock in Novartis. All other authors have no conflict of interest.

turnover (obtained at 2-week to 12-month intervals) were analyzed, with an analysis of covariance model used to assess treatment effect for parameters of interest.

Results and Conclusions—MRI assessment of trabecular microarchitecture at individual regions of the distal radius revealed significant improvement, or preservation (no significant loss), in the CT-NS–treated group compared with significant deterioration in the placebo control group, as reflected in apparent BV/TV ($p < 0.03$), apparent trabecular number ($p < 0.01$), and apparent trabecular spacing ($p < 0.01$). Also, at the hip, the CT-NS group exhibited preservation of trabecular microarchitecture at the lower trochanter ($p < 0.05$) as determined by T2* MRI technology. Significant deterioration of trabecular bone architecture was noted in the placebo group at the femoral neck, Ward's triangle, and lower trochanteric sites. Apart from a significant increase in apparent trabecular number in the CT-NS group, significant changes within or between groups were not noted at the os calcis. Combined μCT/histomorphometric analysis of iliac crest bone biopsies did not reveal significant differences between treated and placebo groups. In the CT-NS group, regardless of the change in BMD (gain or loss) at the spine, hip, or distal radius, preservation of parameters of trabecular microarchitecture was noted, whereas in the placebo group, regardless of the change in BMD (gain or loss) at the spine, hip, or distal radius, loss or preservation was noted; however, changes in DXA/BMD (of the spine, hip, wrist, os calcis) between CT-NS and placebo groups were not significant. Serum C-telopeptide (S-CTx), a specific bone resorption marker, was reduced by 22.5% at 24 months ($p = 0.056$). The results of the QUEST study suggest therapeutic benefit of CT-NS compared with placebo in maintaining trabecular microarchitecture at multiple skeletal sites and support the use of MRI technology for assessment of trabecular microarchitecture in clinical research trials. However, the results also highlight site specific differences in response to antiresorptive therapies and the importance of sufficiently large sampling volumes (areas) to obtain reliable assessment of bone architecture.

Keywords

osteoporosis; salmon calcitonin; magnetic resonance imaging; trabecular microarchitecture; bone quality

INTRODUCTION

Compromised bone quality and bone quantity (as components of bone strength) are recognized as substantially contributing to osteoporotic fracture risk.[1] Perhaps less well recognized is the role of bone quality (including bone architecture, turnover, damage accumulation, material strength, and mineralization) in defining and mediating therapeutic benefit in reducing such fracture risk. However, in this regard, there is increased awareness and an evolving consensus that the reduction in osteoporotic fracture risk in response to certain antiresorptive osteoporosis therapies may be caused less by effects on bone quantity than by effects on bone quality.[2–4] The genesis of such a perhaps heretical concept may have arisen from the results of two previous 3- to 5-year prospective postmenopausal osteoporosis therapy studies, the PROOF trial[5] and the MORE trial,[6] in which relatively modest improvements in spinal BMD were associated with significant reductions in vertebral fracture risk in response to either salmon calcitonin nasal spray (CT-NS)[5] or oral raloxifene,[6] raising questions over the relative contribution of change in bone quantity to

the reduction in fractures seen with these therapeutic agents. Such questions are reinforced with further posthoc analyses of the MORE data,[7] suggesting that only 4% of the vertebral fracture reduction seen with raloxifene in the MORE study was caused by improvement in bone quantity. A second posthoc analysis from the alendronate FIT trial[8] suggests that only 16% of the vertebral fracture reduction in that study was caused by improvement in bone quantity. What might explain the additional reduction in fracture?

A change in bone quality—specifically trabecular microarchitecture—in response to antiresorptive therapy has been hypothesized to explain some proportion of the observed osteoporotic fracture reduction in the previous trials.[2] To test this hypothesis, a 2-year prospective study, the QUEST (Qualitative Evaluation of Salmon Calcitonin Therapy) trial, was conducted in postmenopausal osteoporotic women, using CT-NS as the antiresorptive osteoporosis therapy, with examination of its effects compared with placebo on parameters of bone quantity and bone quality. To assess trabecular microarchitecture as a component of bone quality, the iliac crest bone biopsy with 2D histology,[9] and more recently 3D μCT,[10] has been used. However, the high-resolution MRI technology has shown potential value to noninvasively evaluate trabecular microarchitecture.[11] The QUEST study was designed to determine the effects of CT-NS on trabecular microarchitecture and to evaluate the use of MRI in assessing trabecular structure in prospective clinical trials. We therefore report here the results of the QUEST study, specifically the effects of CT-NS or placebo on trabecular microarchitecture as determined by the relatively unique MRI technology at the radius, hip, and heel (os calcis).

MATERIALS AND METHODS

This double-blind placebo-controlled trial was conducted at a single study site (UWMC–ORG, Seattle, WA, USA).

Study participants

White, Asian, or Hispanic women were eligible to participate if they were postmenopausal for at least 5 years with at least one to five prevalent thoracic or lumbar vertebral compression fractures, a lumbar spine BMD T score of <0, and no history of hip fracture. Women with a history of diseases or receiving medications known to affect bone metabolism were excluded, as were women currently or previously treated with bisphosphonates or currently or previously (within the past 12 months) treated with calcitonin, hormone replacement therapy, selective estrogen receptor modulators (SERMs) such as raloxifene, or PTH. The study protocol was approved by the University of Washington Institutional Review Board, and all women provided written informed consent.

Protocol treatment/follow-up studies

Participants were assigned to receive salmon calcitonin nasal spray at a daily dose of 200 IU (Miacalcin Nasal Spray; Novartis Pharmaceuticals, East Hanover, NJ, USA) or placebo nasal spray, using a computer-generated 1:1 randomization. All participants received one 500 mg calcium carbonate tablet daily. Study subjects were seen at baseline and at months 1, 2, 3, 6, 12, 18, and 24 of the 2-year study. Markers of bone turnover (serum bone-specific

alkaline phosphatase, serum C- and N-telopeptide, urinary N-telopeptide/creatinine) were obtained at baseline, 2 weeks, and 1, 2, 3, 6, 12, and 24 months; lumbar spine, hip, os calcis, and wrist BMD by DXA measurements was obtained at baseline and 1 and 2 years; MRI determinations at wrist, hip, and os calcis were obtained at baseline and 1 and 2 years; and X-rays of the thoracic and lumbar spine, iliac crest bone biopsies, and routine blood hematology/chemistry screening and safety parameters, (hemoglobin, calcium, phosphorus, creatinine, PTH, vitamin D) were obtained at baseline and at 2 years.

Analytical procedures

BMD—BMD was determined at the lumbar spine (L_1–L_4), hip (total hip, femoral neck, Ward's triangle, and tro-chanter sites), os calcis, and nondominant wrist (distal and midcortical sites) by DXA using a Hologic 1500 machine (Waltham, MA, USA); the short-term in vivo precision error for this machine at the UWMC–ORG was <1%.

Spine radiographs—Anterior-posterior (AP) and lateral thoracic and lumbar spine X-rays were evaluated by two of the study investigators (CHC, AS) for the presence of compression fracture; a 20% or greater reduction in anterior height of the individual vertebral body T_3–L_5, compared with posterior height, was accepted as a compression fracture.

Markers of bone turnover—Serum concentrations of bone-specific alkaline phosphatase (a marker of bone formation) were measured with an immunoradiometric assay (Tandem-R Ostase; Hybritech); serum concentrations of C-telopeptide cross-links and serum and urine normalized for creatinine concentrations of N-telopeptide cross-links (markers of bone resorption) were measured with enzyme-linked immunosorbent assays (Crosslaps; Osteometer Biotech and Osteomark; Ostex, respectively). All assays were performed at Pacific Biometrics (Seattle, WA, USA).

MRI—All MRIs (radius, hip, and os calcis; Fig. 1) were acquired using a General Electric Sigma scanner operating at 1.5 T (General Electric Medical Systems, Milwaukee, WI, USA). Images were obtained at the distal radius, using a custom-built phased array coil (University of Washington, Seattle, WA, USA), and the os calcis, using a 5-in surface coil (General Electric Medical Systems). For the radius scans, the patient laid supine with the arm at the side. A coronal, spin-echo localizer was used to identify axial sections starting 7 mm proximal to the joint line and extending into the radial shaft. At these locations, four axial high-resolution fast gradient echo images (Fig. 1A) were obtained at a spatial resolution of 156 μm in-plane and 500 μm in slice direction. The flip angle, echo time, and repetition time were 30°, 5.6 ms, and 29 ms, respectively. The total imaging time for the high resolution scan was 12 minutes.

For the os calcis scans, the patient was also positioned supine; the lateral posterior edge of the foot was restrained, and the foot was rotated by ~20° (range, 10–30°). This was done to ensure that the os calcis was oriented vertically as much as possible, which is necessary for reproducible positioning in the follow-up scans and to assure maximum coverage in the high-resolution scan. An axial locator was used to prescribe a sagittal high-resolution scan

image (195 × 195 × 500 μm) using a 3D gradient echo sequence. The echo time, repetition time, flip angle, and bandwidth were 6.7 ms, 29 ms, 30°, and 7.81 kHz, respectively. At the os calcis, a single region in the posterior location was analyzed (Fig. 1B). The total imaging time was 12 minutes.

For the hip scans, T2* single slice, water-saturated, coronal gradient echo images (resolution 1.875 × 1.875 × 10 mm) were obtained at 12 different echo times ranging from 4 to 40 ms. Four different regions were analyzed: the femoral neck, Ward's triangle, and upper and lower trochanteric regions (Fig. 1C). The relaxation time was determined assuming a monoexponential decay, and the underlying assumption was that the marrow fat T2 relaxation time did not change with therapy. For the T2* relaxation time variable, an increase in T2* relaxation time in milliseconds is viewed as deleterious to bone structure, and a decrease in milliseconds is viewed as beneficial. The total imaging time was 6 minutes.

The MRI scans were transferred to an independent SUN Workstation and processed using software developed in-house based on an IDL (Research Systems, Boulder, CO, USA) interface. For the coil geometries used in this study (radius and os calcis), correction maps based on low-pass-filtered versions of the actual high-resolution images[12] were used to correct the inhomogeneities caused by the coil geometry.

In the radius, an automatic contour tracking algorithm was used to identify the inner rim of cortical shell. An intensity based criterion using the coronal localizer scan was used for the automatic identification of the end plate, as previously described.[13] Regions of interest (ROI) were selected beginning 7 mm from the end plate and extending into the radial shaft, and 2D ROIs defined by the automated identification of the inner cortex were used to determine irregular regions of interest consisting of trabecular bone. A global threshold criterion based on two reference intensity levels, one for marrow fat (I_m) and one for bone (I_b) was used to segment the images.[14] The intensity of the cortical bone was used to define the bone reference I_b as follows: smoothed intensity profiles along rays normal to the cortical bone surface were calculated, and the cortical intensity for each ray was taken as the value of the first minimum outside the trabecular region. The median value from 10 rays was taken as the cortical intensity for a slice. To obtain the final mean bone intensity, these intensity values were averaged for slices >2.5 mm from either end of the analysis region to avoid regions where the cortex was very thin and could lead to errors in the choice of the bone intensity. The marrow reference intensity I_m was automatically selected using the histogram of intensities within the trabecular bone region as previously described.[14] The global threshold was set using the mean intensity of the trabecular region, I_{trab}, to give a bone fraction bone volume/total volume (BV/TV) = $(I_{trab} - I_b)/(I_m - I_b)$. At the os calcis, 10 midsagittal slices (0.5 cm total thickness) were analyzed with the circular ROI. In the os calcis, I_b was selected manually in the background area because the cortical shell is too thin, the marrow intensity was selected as before, and a threshold was set as before.

Stereology techniques for quantifying 3D trabecular bone have been implemented.[15] For this study, the analyses were conducted over a trabecular bone region at the radius and os calcis. Using the segmented binary image the total number of bone pixels in each ROI and

the total area of the ROI were used to compute the apparent BV/TV. The number of pixels that crossed a set of parallel rays at a given angle through the image was counted, and the mean intercept length was computed. The mean intercept length for all angles was used to calculate apparent trabecular number. Apparent trabecular thickness and apparent trabecular spacing were calculated using apparent BV/TV and apparent trabecular number.

The segmented images were also analyzed with the recently introduced[16] 3D distance transformation techniques after the voxels were scaled to an isotropic resolution of 156 μm^3 by replication in the axial direction. Trabecular thickness was assessed by filling the bone phase of the segmented images with maximal spheres and computing the apparent trabecular thickness as the mean diameter of the spheres. Apparent trabecular spacing was measured as the thickness of the marrow spaces. To determine the trabecular number, the trabecular network was skeletonized and the apparent trabecular number was computed as the inverse of the mean distances between the structural elements of the skeleton. The stereology-based and the direct transformation-based techniques for assessing trabecular bone microarchitecture were compared at baseline in this study; significant correlations (R^2 ranging from 0.94 to 0.98 depending on the parameters assessed) were noted between the two techniques. Therefore, in addition to apparent BV/TV, only the stereology-derived measures of apparent trabecular number, spacing, and thickness are reported here.

Reproducibility for the MRI measurements is dependent on image quality for most parameters of trabecular microarchitecture; for seven subjects with reasonable image quality, a reproducibility of 2–4% was found for microstructure parameters.[17]

Bone histology—For histomorphometry and μCT, transiliac crest bone biopsy specimens were obtained from 91 women at baseline (right iliac crest) and from 67 women at the 2-year study conclusion (left iliac crest). Specimens were obtained with a Rochester biopsy trephine (7.5 mm internal diameter; Rochester, MN, USA) after tetracycline hydrochloride was given orally in a 3:12:3-day sequence. Biopsy specimens were fixed in 70% ethanol and forwarded to Dr Erik Eriksen (Bone Histomorphometry Laboratory, Aarhus, Denmark) for analysis.

Standard static 2D histomorphometric parameters for trabecular and cortical bone parameters were measured as previously described.[9,18,19]

After histomorphometric assessment, the nondecalcified specimens, embedded in methyl methacrylate, underwent 3D μCT analysis (Scanco Medical AG, Bassersdorf, Switzerland) as performed by Dr M Glatt (Basle, Switzerland). Parameters obtained included BV/TV, trabecular number, trabecular spacing, and trabecular thickness, as previously described.[20]

Statistical analysis

An analysis of covariance model was used to assess treatment effect for the parameters of interest. The models included a factor indicating treatment group and the baseline value of the parameter of interest as a covariate. All tests were two-sided with a level of significance of 0.05. Given the exploratory nature of the trial, it was specified that no imputation method would be used to account for missing data and that the main analysis would be based on

observed data only. It was also specified that there would be no adjustment made for multiple comparisons. As such, the *p* values presented need to be interpreted in the context of this being an exploratory trial.

RESULTS

One hundred seventy-seven postmenopausal women were screened for the study; 91 were enrolled and randomly assigned to either CT-NS plus calcium ($n = 46$) or placebo nasal spray plus calcium ($n = 45$). The baseline characteristics of the 91 recruited women, including the parameters for microarchitecture, are noted in Tables 1 and 2. No significant differences were noted between treated and control groups for these parameters. All women were at least 5 years postmenopausal, with a lumbar spine T score of <0 and with at least one atraumatic vertebral compression fracture.

Seventy-one of the enrolled 91 women (78%) completed the 2-year study: 33 (72%) in the treated group and 38 (84%) in the placebo control group. Two subjects in the treated group discontinued the study because of nasal events including rhinitis; however, there were no significant differences between treated and control groups in women discontinuing the study. More than 90% of women were >75% adherent to treatment during their study participation, as determined by assessment of remaining drug in the nasal spray canister at study visits.

Ninety-one and 66 women provided baseline and 2-year MRI scans, respectively; reasons for declining the MRI procedure at wrist, hip, and/or heel included claustrophobia ($n = 3$) or inability to remain stationary for the entire procedure ($n = 2$). Specifically, 66 scan sets from the 71 women completing the study were forwarded to the UCSF group (SM, DCN) for analysis. Overall, no MRI images were eliminated for motion- or image quality-based considerations once received and analyzed by the UCSF group. However, four hip scans were analyzed but were not used in the study data analysis because of positioning at an incorrect site at follow-up compared with baseline. For the wrist scans, incorrect positioning of the wrist for the follow-up scans resulted in the deletion from study data analysis of 12 scan sets at region 1, 8 scan sets at region 2, 6 scan sets at region 3, and 4 scan sets at region 4. For region 4, an additional 10 scan sets were deleted from study data analysis because of incorrect coil placement, for a total of 14 scan sets deleted at region 4.

MRI results: radius

At baseline, correlations of BMD as determined by DXA and trabecular microarchitecture parameters as determined by MRI were assessed. At the radius, correlations were modest but significant ($p < 0.05$) and were dependent on the region (ultradistal or distal BMD, and regions 1–4 MRI): for apparent bone volume/total volume, the correlation coefficients ranged from 0.42 to 0.57, for apparent trabecular number the correlation coefficients ranged from 0.34 to 0.51, and for apparent trabecular spacing the correlation coefficients ranged from –0.26 to –0.47. For the os calcis, the correlations between DXA-assessed BMD and apparent bone volume/total volume, apparent trabecular number, and spacing were 0.42, 0.37, and –0.39, respectively ($p < 0.05$). Correlations between BMD and apparent trabecular thickness were not significant for either radius or os calcis. At the hip, T2* correlations were

again dependent on the MRI hip region, but for total hip BMD ranged from –0.26 to –0.58, and –0.33 to –0.55 for femoral neck BMD ($p < 0.05$) Such correlations are similar to those previously noted.[11,21]

Correlations of apparent bone volume/total volume (apparent BV/TV) to the other radial trabecular microarchitecture parameters were assessed at baseline to determine the relationship of apparent BV/TV to apparent trabecular number/ spacing/thickness. The correlations between apparent BV/TV and the other parameters were significant ($p < 0.05$) and ranged from moderate to good (e.g., for region 2 of the radius, the correlation between apparent BV/TV and apparent trabecular number/spacing/thickness was 0.87, –0.85, and 0.44, respectively; for region 3, the correlations were 0.89, –0.90, and 0.60, respectively).

High-resolution MRI assessment of trabecular microarchitecture at four regions of the distal radius through 2 years revealed a significant 2% percent gain in apparent trabecular bone volume (BV/TV) at region 1 within the CT-NS–treated group, with no significant change at region 1 in the placebo control group (+0.3%; Table 3). Significant percentage losses of –5.9% and –9.1% at regions 3 and 4 were observed in the placebo control group, whereas no significant changes from baseline were seen for the CT-NS group at these regions (–0.5% and +0.4%, respectively). Significant differences between treated and control groups in percent change in apparent BV/TV through 2 years were seen at regions 3 (5.4%) and 4 (9.8%; Fig. 2A; Table 3).

A significant increase (+1.7%) in apparent trabecular number and a significant decrease (–2.3%) in apparent trabecular spacing were noted at region 1 within the CT-NS– treated group; significant decreases in apparent trabecular number (–4.1% and –6.9%) and significant increases in apparent trabecular spacing (+8.8% and +12.9%) were found at regions 3 and 4, respectively, in the placebo control group. There were significant differences in percent change through 2 years between treated and control groups for apparent trabecular number (5.1% and 8.9%) and apparent trabecular spacing (–8.8% and –13.8%) at regions 3 and 4, respectively, and borderline significant differences in apparent trabecular number at region 1 ($p = 0.050$; Figs. 2B and 2C; Table 3).

For apparent trabecular thickness, significant losses from baseline were noted in the placebo control group at regions 3 and 4 (Fig. 2D; Table 3), but no between-treatment group differences were shown.

Absolute changes were in agreement with percent changes in CT-NS–treated and placebo control groups across regions 1–4 for all measured parameters, except for absolute change in apparent BV/TV in the NS-CT group at region 1 ($p = 0.09$ for absolute change, $p = 0.03$ for percent change). MRI scans were also obtained at 12 months of study participation; changes at 12 months within and between treated and placebo control groups for all MRI parameters at all regions of the distal radius showed similar trends to those seen at 24 months, but were not significant except for apparent BV/TV that increased at region 1 in the CT-NS–treated group ($n = 32$; +2.49%; 95% CI, 0.04, 4.94; $p = 0.047$) and for apparent trabecular spacing that, in the placebo group, worsened at region 3 ($n = 35$; +6.34%; 95% CI, 1.21, 11.48; $p = 0.016$; data not shown).

To address potential concerns regarding the variable responses to CT-NS or placebo across the individual regions 1–4, average absolute and percentage changes within and between treated and placebo groups were examined by calculating the mean for each structural parameter across the four regions at baseline and 12 and 24 months, with a percentage change calculated based on the means. Again, significant losses (save for apparent trabecular thickness) were noted within the placebo group (apparent BV/TV, –4.51%, p = 0.002; apparent trabecular number, –4.03%, p = 0.002; apparent trabecular spacing, +10.72%, p = 0.003; apparent trabecular thickness, –1.11%, p = 0.138). Such losses were significantly different (save for apparent trabecular thickness) between the treated and placebo groups (apparent BV/TV, +5.67%, p = 0.005; apparent trabecular number, +5.43, p = 0.002; apparent trabecular spacing, –11,56%, p = 0.004; apparent trabecular thickness, +0.64%, p = 0.531). No significant average within group changes were noted in the parameters of the treated group; the significant gains in apparent BV/TV and apparent trabecular number/spacing noted in the treated group at region 1 were not seen when the means of regions 1–4 were assessed.

MRI results: hip

Significant percent increases through 2 years in MRI-derived T2* relaxation times were noted in the placebo control group at the femoral neck, Ward's triangle, and lower trochanteric sites of the proximal femur and in the CT-NS treated group only at the Ward's triangle site; again, an increase in T2* relaxation time reflects a deleterious effect on bone structure. Changes between treated and control groups were significantly different only at the lower trochanteric site (–7.42%; 95% CI, –12.49, –2.34; p = 0.049; Fig. 3).

MRI results: os calcis

There was a statistically significant increase in apparent trabecular number at the os calcis in the CT-NS–treated group (+1.66%; 95% CI, 0.61, 2.72; p = 0.003; data not shown). The remainder of the parameters were not statistically significantly different from placebo.

Relationship between change in trabecular microarchitecture and change in BMD in response to therapy

To examine the relationships between changes in MRI-derived microarchitectural parameters and changes in DXA-derived BMD in response to CT-NS or placebo, dichotomous analyses were performed. Subjects were divided into those women gaining BMD/showing no change and losing BMD at the spine, hip, or distal radius. Percentage changes in MRI microarchitectural parameters at the distal radius and hip were computed for treated and control groups gaining or losing BMD at the spine, hip, or distal radius (Table 4; Fig. 4). Although for MRI parameters the region 4 site of the distal radius and the femoral neck and lower trochanteric hip regions showed the most significant findings (Table 4; Fig. 4), the relationships noted in Table 4 and Fig. 4 between change in microarchitecture and change in BMD were consistent for other distal radius and hip sites across all MRI measurements.

As noted in Table 4 and Fig. 4, women in the placebo control group losing BMD at the lumbar spine, hip, or distal radius were significantly losing trabecular microarchitecture at

the distal radius (region 4) and at the femoral neck and lower trochanteric sites of the hip (as implied by an increase in the T2* measurement). However, women in the CT-NS–treated group, even though losing BMD at the spine, hip, or distal radius, showed a consistent preservation (no significant loss) of trabecular microarchitecture at these skeletal sites. Also, these changes between the treated and control groups losing spine or total hip BMD were significantly different at the radius (save for trabecular thickness; Table 4), at the femoral neck of the hip (Table 4; Fig. 4) and at the lower trochanter of the hip ($p = 0.05$; Fig. 4). However, in women receiving placebo and gaining/no change in BMD at the spine or total hip, significant deterioration in trabecular microarchitecture was noted at the lower trochanteric and Ward's triangle hip site (+10.2% and + 12.8%, respectively, for gain in spine BMD; Table 4; and +10.0% at the lower trochanteric site for gain in total hip BMD; Fig. 4).

At region 3 of the distal radius, significant losses were noted in apparent trabecular number (–3.13 ± 4.38%; $p < 0.02$) and significant increases were noted in apparent trabecular spacing (+6.16 ± 8.88%; $p < 0.03$) in the placebo group women gaining/showing no change in BMD at the spine; such changes were significantly different from women in the treated groups (data not shown).

Relationships between changes in BMD/MRI and changes in MRI/MRI at different skeletal sites

Across the entire cohort of treated and placebo groups, for most sites, the correlations between changes in spine or hip BMD and changes in MRI parameters at the forearm or hip were nonsignificant (Table 5), as were the changes in MRI parameters at different skeletal sites (Table 6). However, the correlations between midradius BMD and MRI parameters of distal radius regions 3 and 4 reached significance for apparent BV/TV (Table 5), apparent trabecular number (region 3: $r = 0.312$, $p = 0.015$; region 4: $r = 0.331$. $p = 0.017$), and apparent trabecular spacing (region 3: $r = –0.356$, $p = 0.005$; region 4: $r = –0.429$, $p = 0.002$; data not shown). When correlating MRI parameters from the four regions of the forearm to T2* MRI parameters of the hip, apparent BV/TV at region 4 of the distal radius reached significance ($p < 0.05$) at the femoral neck and upper tro-chanter of the hip (Table 6).

BMD results

No significant changes (percent or absolute) were noted through 2 years within or between CT-NS–treated and placebo groups in BMD at spine, hip, wrist, or os calcis (spine BMD + 0.84% difference compared with placebo, median reported because of skewness of data).

Bone turnover marker results

Serum C-telopeptide (CTx) showed a 22.5 ± 11.8% (SE) difference compared with placebo at 2 years ($p = 0.056$). If the statistical analysis was performed as the last observation carried forward, the reduction was –25.3% ($p = 0.02$). No significant changes in serum or urine N-telopeptide (NTx) or serum bone-specific alkaline phosphatase (BSALP) were noted in the treated or control groups.

Blood safety parameters/spine X-ray results

No abnormalities of blood safety parameters were noted; two new spinal fractures were noted in each group during the study.

Iliac crest bone biopsy results: histomorphometry and μCT

No significant changes in histomorphometric or μCT parameters were noted at 2 years, compared with baseline, within or between the treated and control groups, except for a significant difference in mean resorption rate as determined histomorphometrically (–0.399 ± 0.253 μm/day NS-CT, 0.380 ± 0.285 μm/day placebo, $p < 0.048$).

A detailed report of the iliac crest bone biopsy results (histomorphometry and μCT) and the relationships of these results to changes in BMD, markers of bone turnover, and MRI parameters will be the subject of a separate communication.

DISCUSSION

This study is the first clinical trial designed a priori to prospectively examine and compare the effects of an anti-resorptive osteoporosis therapy, in this study, salmon calcitonin nasal spray, specifically on parameters of trabecular microarchitecture, using both noninvasive MRI technology and invasive iliac crest bone biopsy–based μCT/ histomorphometry techniques to assess trabecular structure. The study shows significant preservation and/or improvement of trabecular microarchitecture (as determined by high-resolution MRI measurements of apparent bone volume/total volume, trabecular number, and trabecular spacing) at the distal radius in the postmenopausal osteoporotic women receiving CT-NS and calcium over 2 years compared with significant deterioration of trabecular microarchitecture in the women receiving only calcium. Preservation of bone quantity and structure, as measured by the MRI measurement of T2* relaxation time, was noted in the CT-NS group at the femoral neck and trochanteric regions of the proximal femur; significant deterioration (an increase in milliseconds) of this T2* relaxation time parameter was noted at multiple proximal femur sites in the calcium only control group. CT-NS–treated and control group subjects were stratified into groups gaining or losing BMD through 2 years at the spine, hip, or distal radius with subsequent examination of changes in the MRI-derived microarchitecture parameters in these groups. Women receiving CT-NS preserved trabecular microarchitecture at the distal radius and hip, regardless of their change in BMD (gain or loss): as noted in Table 4 and Fig. 4, no significant losses were noted in the CT-NS group in terms of parameters of trabecular microarchitecture even in those women in whom BMD was decreasing. However, significant losses of parameters of trabecular microarchitecture were noted at the wrist and hip in the placebo group losing BMD at the spine, hip, or distal radius. Such observations in the CT-NS treated group suggest a discordance between change in bone mineral quantity (as measured by BMD) and change in bone quality (as defined by trabecular microarchitecture), in response to the antiresorptive osteoporosis therapy salmon calcitonin, as hypothesized previously.[2] Although osteoporotic fracture was not an endpoint in this study, such discordance might contribute to an understanding of the apparent paradox in a number of clinical trials[5,6] of fracture reduction with only modest improvements in BMD, i.e., an effect on bone quality rather than bone quantity to explain

the observed reduction in osteoporotic fracture risk. Also, at the lower trochanteric and Ward's triangle regions of the femur and at region 3 of the distal radius, significant deterioration was noted in parameters of trabecular microarchitecture (T2* relaxation time, and apparent trabecular number and spacing) in the calcium-only placebo group, even in those women who were gaining or showing no change in BMD at the spine or hip or distal radius. Such observations, whereas admittedly in small subgroups (14–16 subjects), raise questions regarding the adequacy of calcium supplementation (500 mg daily) alone to preserve trabecular microarchitecture in elderly postmenopausal osteoporotic women who are maintaining or even increasing BMD at the spine or hip.

Few previous studies in humans have been designed primarily to explain the effects of osteoporosis therapies, antiresorptive or bone-forming, on trabecular microarchitecture. Studies that have been performed have, most frequently, been substudies of larger clinical trials and have used paired iliac crest bone biopsies with 2D histomorpho-metric analysis of the biopsy specimens, with only recently the application of the μCT technique for a more specific 3D assessment of iliac crest trabecular microarchitecture. In response to estradiol[22] or estradiol/norethisterone[23] therapy, no significant change in BV/TV, and either no significant change[23] or a decrease[22] in wall thickness, was noted after paired iliac crest bone biopsy histomorpho-metric analysis in 22–28 postmenopausal osteopenic or osteoporotic women studied for 1–2 years. In response to bisphosphonate treatment, preservation of trabecular microarchitecture (BV/TV, trabecular number and spacing, trabecular thickness, and connectivity density), similar to that seen at the radius and hip in this study, was noted in 14 postmenopausal osteopenic women in response to 1 year of risedronate treatment as determined by μCT analysis of paired iliac crest bone biopsy specimens[24]; in 12 placebo control subjects significant deterioration of these microarchitecture parameters was noted. In response to alendronate therapy, a preliminary report[25] postulated an increase in BV/TV, trabecular number and thickness, and connectivity as determined by both iliac crest biopsy histomorphometric and μCT analysis in 14 osteoporotic women followed for 2 years, but the study only considered single end-of-study biopsy specimens, as did a previous study suggesting a significant increase in the histomorphometry determined wall thickness.[26] For anabolic bone-forming therapies such as PTH, an interestingly little significant effect on the trabecular microstructural parameters of number, spacing, and thickness was noted in two studies: one was an uncontrolled study in 16 individuals (females and males) treated for 1.5–3 years with recombinant PTH(1-34),[27] and the other was a placebo-controlled substudy of the effects of 19 months of teriparatide in postmenopausal osteoporotic women (n = 51).[19] Both studies used paired iliac crest bone biopsy with histomorphometric and μCT analysis techniques. Significant improvement in μCT determined connectivity density in response to PTH therapy was noted in both studies.[19,27] Jiang et al.[19] noted a significant improvement after teriparatide therapy in structure model index and cortical thickness. In the same study, BV/TV, as determined histomorphometrically, exhibited a significant increase. This increase was, however, not demonstrable with μCT, revealing a discrepancy between X-ray–based assessment of bone mineral (μCT) and histomorphometric assessment of stainable bone tissue. Additionally, studies using paired biopsies from both sides of the ilium are confounded by significant error caused by an intrabone variation of 30% between sides[28]

and the small sample size, demanding rather large number of biopsies to achieve sufficient power.

Some of these problems could conceivably be overcome by longitudinal QCT or MRI imaging of the same bone site, provided sufficient resolution could be achieved. These techniques can assess the same bone area repeatedly and can also sample from larger volumes (or areas) than those achievable with bone biopsies. A secondary aim of the QUEST study was therefore to evaluate the use of MRI for assessing trabecular structure in clinical trials, and specifically in noninvasively determining the effects of osteoporosis therapies on the trabecular microarchitecture of bone. Because the microarchitectural structure of trabecular bone may play a significant role in determining biomechanical bone strength,[29] such use of MRI measurements may be of value not only for defining osteoporotic fracture risk and therapeutic response in research studies, but also potentially for determination of clinical response to osteoporosis treatment beyond that currently available with DXA (BMD), bone turnover markers, and/or skeletal X-ray.

MRI currently uses two different in vivo approaches for assessment of trabecular bone microstructure. First is a “direct” depiction of the trabecular network with high-resolution MRI followed with image analysis; a limitation includes the resolution achievable, with subsequent partial volume effects.[30] Image analysis may be based on extracting measures synonymous with histomorphometric measurements such as trabecular number, spacing, and thickness, based on whether a plate model or direct assessment of microstructure is used.[10] In addition, images may also be analyzed using a digital topological analysis (DTA) of magnetic resonance microimages with a subsequent assessment of the 3D topology of each voxel.[31] Whereas trabecular bone architecture is complex, anisotrophic, and displays considerable variability across skeletal sites,[10,30] the relationship between MRI-derived trabecular structure and biomechanical integrity of trabecular bone has been well established both in vitro and in vivo with these approaches.[11,15,29,32] As well, preliminary results from an on going study[33] suggests the DTA methodology may assess the effect of estrogen on trabecular microarchitecture at the wrist.

The second MRI-based methodology is an “indirect” assessment of bone quality through a measurement of the T2* decay rate of marrow, assessing bone quantity, the overall trabecular architecture, and the orientation of trabeculae.[30]

For determining the therapeutic effects of CT-NS on trabecular microarchitecture, the QUEST study used both the direct characterization of the trabecular network by HRMRI at the radius and heel and the indirect T2* MRI methodology at the hip. As confirmed in this study, MRI advantages include its noninvasive nature, its 3D assessment of bone structure, its capability for assessing multiple skeletal sites, its lack of exposure to ionizing radiation, and in general, its acceptability to research subjects. Whereas shortcomings of the MRI procedure include length of time of the procedure, the occasional claustrophobia associated with the closed MRI scanner, and the partial volume effects on measurement of certain trabecular structure parameters (trabecular thickness), such shortcomings may be obviated with future MRI technical advances. Overall, the study suggests that the MRI technology

may provide a research, and potentially a clinical, alternative to the more traditional, but invasive, iliac crest bone biopsy for assessing trabecular structure.

A number of questions are raised by the results of the study. First, the size of the study (n = 91) prohibits reaching any conclusions regarding the effects on fracture reduction of such apparent trabecular microarchitecture preservation after CT-NS therapy. However, a relationship between trabecular microarchitecture and biomechanical integrity and osteoporotic fracture risk has been postulated[34,35] and confirmed in vitro[15,29,32,36] and in vivo.[37] As well, a recent paper[38] has noted a significant effect of salmon calcitonin on compressive stress in an animal model. It may therefore be hypothesized that preservation of trabecular microarchitecture will translate into a reduced fracture risk, but larger multicenter clinical trials using MRI measurements, with fracture as an endpoint, are necessary to confirm such a hypothesis (this study was a single-site exploratory study).

A second question is the variable therapeutic response to CT-NS, in terms of trabecular microarchitecture, and for the various methodologies (MRI, DXA, bone turnover markers, etc.) used in this study. The MRI-derived trabecular microarchitecture results note disparities in terms of therapeutic response within (regions 1–4 at the radius and the proximal femoral sites) and between (radius, hip, os calcis) the measured skeletal sites; iliac crest biopsy–derived histomorphometric and μCT results differ from those obtained with MRI. However, a differential, heterogeneous therapeutic response (improvement at one skeletal site, no change or loss at another skeletal site) has been noted in previous osteoporosis therapy trials in terms of BMD change at spine/hip/wrist[6,39] and in terms of fracture.[6] A similar site-specific therapeutic response for trabecular microarchitecture would not be unexpected and may be caused not only by differing amounts of cortical and trabecular bone at different skeletal sites such as has been seen at the distal radius by Majumdar et al.[40] but also as shown by Hildebrand et al.[10] to differing types of trabecular bone at these sites (i.e., rods, plates, and rods and plates combined). There may be quantitative differences in trabecular microstructure within the same skeletal site as shown by Thomsen et al.[41] at the vertebrae. Differential changes in response to CT-NS treatment, or placebo, within the regions 1–4 at the radius, or between the radius, hip, and os calcis, may therefore be caused by such microarchitectural heterogeneity; in this regard, it is also worth noting that the sampling of MRI slices of the radius in this study traversed areas with very different mechanical strain distributions, as shown by finite element analysis.[42] These differences may also partly account for the heterogeneous response to CT-NS seen in the four regions of the radius. The significant correlations shown in Tables 5 and 6 between forearm BMD, different MRI areas of the hip, and MRI regions 3 and 4 of the forearm would, however, suggest that the changes seen in these regions of the distal radius better reflect overall skeletal response than do regions 1 or 2. Last, the apparent lack of histomorphometric and μCT response to CT-NS at the iliac crest (no significant change within or between treatment and placebo groups) is also not totally unexpected, again because of microarchitectural heterogeneity of therapeutic response across differing skeletal sites.

In terms of a lack of a statistically significant therapeutic effect on BMD/DXA at multiple skeletal sites and the lack of concordance of BMD change with MRI trabecular

microarchitecture change (although across the entire treated and control cohort, significant correlations were noted at regions 3 and 4 of the radius; Table 5), a likely explanation is a masking of potential therapeutic effects of CT-NS by superimposed cortical components included in the projectional DXA measurement (which integrates cortical and trabecular bone, whereas MRI measures purely trabecular bone); CT-NS may primarily affect trabecular bone rather than cortical bone. In this regard, trabecular BV/TV as measured by histomorphometry, μCT or MRI correlates strongly to site-matched trabecular BMD as determined by QCT or mCT; in this study, a significant relationship is noted at baseline between MRI apparent BV/TV at the radius and radial BMD/DXA and is noted between change in MRI apparent BV/TV at the radius and radial BMD, although only at regions 3 and 4 (Table 5).

In terms of the effect on bone turnover markers, CT-NS caused a 22.5% decrease in bone turnover as assessed by serum CTx. This decrease was of borderline significance ($p = 0.056$). Previous studies[43,44] have indicated that CT-NS exerts significant effects on serum CTx: Srivastava et al.[43] reported reductions ranging between 22% and 34%, and Zikan and Stepan[44] noted a 55% reduction in bone resorption as determined by serum CTx 1–3 h after CT-NS administration. The reductions in this study are within the same range, albeit of only borderline significance. Although all efforts were made to standardize the time of blood sample collections (early morning), it is quite possible that disparities in time of collection may have contributed to variability in therapeutic response. The lack of reduction in NTx and bone-specific alkaline phosphatase after CT-NS is in line with previous reports.[45] The presence of inhibition of bone resorption with limited effect on bone formation has also been shown with oral calcitonin.[46]

A third question is an apparent anabolic effect of CT-NS on trabecular microarchitecture (significant improvement in apparent BV/TV, and apparent trabecular number and spacing, at region 1 of the radius, but not when the means of regions 1–4 were assessed). Whereas Farley et al.[47] and Furuichi et al.[48] have suggested in vitro, or in vivo animal, effects of CT-NS on bone formation, such findings have been relatively unique, and a possible anabolic effect remains hypothetical. The specific mechanism for the apparent improvement in microarchitecture is therefore unclear, but nevertheless the finding is statistically significant.

The results of the QUEST study therefore suggest therapeutic benefit of CT-NS compared with placebo in maintaining trabecular microarchitecture at multiple skeletal sites, as determined by the MRI technology. As well, the use of MRI for assessment of trabecular microarchitecture in clinical research trials is supported by these results. Interestingly, and perhaps paradoxically, such therapeutic benefit is achieved in the absence of an effect on BMD/DXA and at the iliac crest. However, the results also highlight site-specific differences in response to antiresorptive therapies and the importance of sufficiently large sampling volumes (areas) to obtain reliable assessment of bone architecture.

ACKNOWLEDGMENTS

This study was funded by grants from Novartis Pharmaceuticals. P Pitzel, RN, J Kaiser RN, and S Danielson contributed to the clinical and administrative care of the research subjects. The participation of the research subjects was exemplary and much appreciated.

REFERENCES

1. National Institutes of Health (NIH). Consensus Development Panel 2000 Osteoporosis Prevention, Diagnosis, and Therapy.. NIH Consensus Statement. 2001. Available online at http://consensus.nih.gov. Accessed
2. Chesnut CH, Rosen CJ. Reconsidering the effects of antiresorptive therapies in reducing osteoporotic fracture (Perspective). J Bone Miner Res. 2001; 16:2163–2172. [PubMed: 11760829]
3. Delmas PD. How does antiresorptive therapy decrease the risk of fracture in women with osteoporosis? Bone. 2000; 27:1–3. [PubMed: 10865202]
4. Riggs BL, Melton LJ. Bone turnover matters: The raloxofene paradox of dramatic decreases in vertebral fractures without commensurate increases in bone density. J Bone Miner Res. 2002; 17:11–14. [PubMed: 11771656]
5. Chesnut CH, Silverman S, Andriano K, Genant HK, Gimona A, Harris S, Kiel D, LeBoff M, Maricic M, Miller P, Moniz C, Peacock M, Richardson P, Watts N, Baylink D. A randomized trial of nasal spray salmon calcitonin in postmenopausal women with established osteoporosis: The Prevent Recurrence of Osteoporotic Fracture study. Am J Med. 2000; 109:267–276. [PubMed: 10996576]
6. Ettinger B, Black DM, Mitlak BH, Knickerbocker RK, Nick-elsen T, Genant HK, Christiansen C, Delmas PD, Zanchetta JR, Stakkestad J, Gluer CC, Krueger K, Cohen FJ, Eckert S, Ensrud KE, Avioli LV, Lips P, Cummings SR. Reduction of vertebral fracture risk in postmenopausal women with osteoporosis treated with raloxifene. JAMA. 1999; 282:637–645. [PubMed: 10517716]
7. Sarkar S, Mitlak BH, Wong M, Stock JL, Black DM, Harper KD. Relationships between bone mineral density and incident vertebral fracture risk with raloxifene therapy. J Bone Miner Res. 2002; 17:1–10. [PubMed: 11771654]
8. Cummings SR, Karpf DB, Harris SF, Genant HK, Black DM. Improvement in spine bone density and reduction in risk of vertebral fractures during treatment with anti-resorptive drugs. Am J Med. 2002; 112:281–289. [PubMed: 11893367]
9. Parfitt AM, Drezner MK, Glorieux FH, Kanis JA, Malluche H, Meunier PJ, Ott SM, Recker RR. Bone histomorphometry: Standardization of nomenclature, symbols, and units. Report of the ASBMR Histomorphometry Nomenclature Committee. J Bone Miner Res. 1987; 2:595–610. [PubMed: 3455637]
10. Hildebrand T, Laib A, Muller R, Dequeker J, Ruegsegger P. Direct three-dimensional morphometric analysis of human cancellous bone: Microstructural data from spine, femur, iliac crest and calcaneus. J Bone Miner Res. 1999; 14:1167–1174. [PubMed: 10404017]
11. Newitt DC, Majumdar S, van Rietbergen B, von Ingersleben G, Harris ST, Genant HK, Chesnut C, Garnero P, MacDonald B. In vivo assessment of architecture and micro-finite element analysis derived indices of mechanical properties of trabecular bone in the radius. Osteoporos Int. 2002; 13:6–17. [PubMed: 11878456]
12. Wald LL, Carvajal L, Moyher SE. Phased array detectors and an automated intensity-correction algorithm for high-resolution MR imaging of the human brain. Magn Reson Med. 1995; 34:433–439. [PubMed: 7500883]
13. Newitt, D.; Majumdar, S. A Semi-Automated System for Segmenting, Registering, Thresholding, and Analyzing High Resolution MRI of Trabecular Bone.. Proceedings of the 8th Annual Meeting of the ISMRM 2000; Denver, Colorado. 2000.
14. Majumdar S, Genant HK, Grampp S, Newitt DC, Truong VH, Lin JC, Mathur A. Correlation of trabecular bone structure with age, bone mineral density, and osteoporotic status: In vivo studies in the distal radius using high resolution magnetic resonance imaging. J Bone Miner Res. 1997; 12:111–118. [PubMed: 9240733]

15. Majumdar S, Kothari M, Augat P, Newitt DC, Link TM, Lin JC, Lang T, Lu Y, Genant HK. High-resolution magnetic resonance imaging: Three-dimensional trabecular bone architecture and biomechanical properties. Bone. 1998; 22:445–454. [PubMed: 9600777]
16. Hildebrand T, Ruegsegger P. A new method for the model independent assessment of thickness in three-dimensional images. J Microsc. 1997; 185:245–246.
17. Newitt D, van Rietbergen B, Majumdar S. Processing and analysis of in vivo high-resolution MR images of trabecular bone for longitudinal studies: Reproducibility of structural measures and micro-finite element analysis derived mechanical properties. Osteoporos Int. 2002; 13:278–287. [PubMed: 12030542]
18. Eriksen EF. Normal and pathological remodeling of human trabecular bone: Three dimensional reconstruction of the remodeling sequence in normals and in metabolic bone disease. Endocr Rev. 1986; 7:379–408. [PubMed: 3536460]
19. Jiang Y, Zhao JJ, Mitlak BH, Wang O, Genant HK, Eriksen E. Recombinant human parathyroid hormone (1-34) (Teriparatide) improves both cortical and cancellous bone structure. J Bone Miner Res. 2003; 18:1932–1941. [PubMed: 14606504]
20. Jiang, Y.; Zhao, J.; Genant, HK. Macro and micro imaging of bone architecture.. In: Bilezikian, JP.; Raisz, LG.; Rodan, GA., editors. Principles of Bone Biology. 2nd ed.. Academic Press; San Diego, CA, USA: 2002. p. 1599-1623.
21. Majumdar S, Link TM, Augat P, Lin JC, Newitt D, Lu Y, Lane NE, Genant HK. Trabecular bone architecture in the distal radius using magnetic resonance imaging in subjects with fractures of the proximal femur. Osteoporos Int. 1999; 10:231–239. [PubMed: 10525716]
22. Vedi S, Compston JE. The effects of long-term hormone replacement therapy on bone remodeling in postmenopausal women. Bone. 1996; 19:535–539. [PubMed: 8922654]
23. Steiniche T, Hasling C, Charles P, Eriksen EF, Mosekilde L, Melsen F. A randomized study on the effects of estrogen/ gestagen or high dose oral calcium on trabecular bone remodeling in postmenopausal osteoporosis. Bone. 1989; 10:313–320. [PubMed: 2690898]
24. Dufresne TE, Chmielewski PA, Manhart MD, Johnson TD, Borah B. Risedronate preserves bone architecture in early postmenopausal women in 1 year as measured by three-dimensional microcomputed tomography. Calcif Tissue Int. 2003; 73:423–432. [PubMed: 12964065]
25. Masarachia P, Howard T, Santora A, Yates J, Rodan GA, Recker RR, Kimmel DB. Alendronate increases trabecular bone connectivity in elderly osteoporotic women. J Bone Miner Res. 2003; 18:S2–S372. [PubMed: 14601618]
26. Chavassieux PM, Arlot ME, Reda C, Wei L, Yates JA, Meunier PJ. Histomorphometric assessment of the long-term effects of alendronate on bone quality and remodeling in patients with osteoporosis. J Clin Invest. 1997; 100:1475–1480. [PubMed: 9294113]
27. Dempster DW, Cosman F, Kurland ES, Zhou H, Nieves J, Woelfert L, Shane E, Plavetic K, Muller R, Bilezikian J, Lindsay R. Effects of daily treatment with parathyroid hormone on bone microarchitecture and turnover in patients with osteoporosis: A paired biopsy study. J Bone Miner Res. 2001; 16:1846–1853. [PubMed: 11585349]
28. Melson F, Melson B, Mosekilde L. An evaluation of the quantitative parameters applied in bone histology. Acta Pathol Microbiol Scand. 1978; 86:63–69.
29. Ulrich D, van Rietbergen B, Laib A, Ruegsegger P. The ability of three-dimensional structural indices to reflect mechanical aspects of trabecular bone. Bone. 1999; 25:55–60. [PubMed: 10423022]
30. Beuf O, Newitt DC, Mosekilde L, Majumdar S. Trabecular structure assessment in lumbar vertebrae specimens using quantitative magnetic resonance imaging and relationship to mechanical competence. J Bone Miner Res. 2001; 16:1511–1519. [PubMed: 11499874]
31. Wehrli FW, Gomberg BR, Saha PK, Song HK, Hwang SN, Snyder PJ. Digital topological analysis of in vivo magnetic resonance microimages of trabecular bone reveals structural implications of osteoporosis. J Bone Miner Res. 2001; 16:1520–1531. [PubMed: 11499875]
32. Link TM, Majumdar S, Lin JC, Newitt D, Augat P, Ouyang A, Mathur A, Genant HK. A comparative study of trabecular bone properties in the spine and femur using high resolution MRI and CT. J Bone Miner Res. 1998; 13:122–132. [PubMed: 9443798]

33. Wehrli FW, Popescu AM, Vasilic B, Gomberg BR, Saha PK, Zemel B, Bunker B, Wright AC, Snyder PJ, Peachy H. Longitudinal changes in trabecular bone architecture detected by micro-MRI based virtual bone biopsy. J Bone Miner Res. 2003; 18:S2–S27. [PubMed: 14601618]
34. Parfitt AM. Implications of architecture for the pathogenesis and prevention of vertebral fracture. Bone. 1992; 13:S41–S47. [PubMed: 1627414]
35. Kleerekoper M, Villanueva AR, Stanciu J, Rao DS, Parfitt AM. The role of three-dimensional trasbecular microstructure in the pathogenesis of vertebral compression fractures. Calcif Tissue Int. 1985; 37:594–597. [PubMed: 3937580]
36. Ciarelli TE, Fyhrie DP, Schaffler MB, Goldstein SA. Variations in three-dimensional cancellous bone architecture of the proximal femur in female hip fractures and in controls. J Bone Miner Res. 2000; 15:32–40. [PubMed: 10646112]
37. Legrand E, Chappard D, Pascaretti C, Duquenne M, Krebs S, Rohmer V, Basle M-F, Audran M. Trabecular bone microarchitecture, bone mineral density, and vertebral fractures in male osteoporosis. J Bone Miner Res. 2000; 15:13–19. [PubMed: 10646109]
38. Jiang Y, Zhao J, Geusens P, Liao E-Y, Andriaensens P, Gelan J, Azria M, Boonen S, Caulin F, Lynch JA, Ouyang X, Genant HK. Femoral neck trabecular microstructure in ovariectomized ewes treated with calcitonin: MRI microscopic evaluation. J Bone Miner Res. 2005; 20:125–130. [PubMed: 15619678]
39. Black DM, Cummings SR, Karpf DB, Cauley JA, Thompson DE, Nevett MC, Bauer DC, Genant GK, Haskell WL, Marcus R, Ott SM, Torner JC, Quandt SA, Reiss TF, Ensrud KE. Randomised trial of effect of alendronate on risk of fracture in women with existing vertebral fractures. Lancet. 1996; 348:1535–1541. [PubMed: 8950879]
40. Majumdar S, Genant HK, Grampp S, Newett DC, Truong VH, Lin JC, Mathur A. Correlations of trabecular bone structure with age, bone mineral density, and osteoporotic status: In vivo studies in the distal radius using high resolution magnetic resonance imaging. J Bone Miner Res. 1997; 12:111–118. [PubMed: 9240733]
41. Thomsen JS, Ebbeson EN, Mosekilde L. Zone-dependent changes in human vertebral trabecular bone: Clinical implications. Bone. 2002; 30:664–669. [PubMed: 11996902]
42. Pistoia W, Van Rietbergen B, Lochmuller E-M, Lill CA, Eckstein F, Ruegsegger P. Estimation of distal radius failure load with micro-finite element analysis models based on three-dimensional peripheral quantitative computed tomography images. Bone. 2002; 30:842–846. [PubMed: 12052451]
43. Srivastava AK, Libanati C, Hohmann O, Kriegman A, Baylink DJ. Acute effects of calcitonin nasal spray on serum serum C-telopeptide of type 1 collagen (CTx) levels in elderly osteopenic women with increased bone turnover. Calcif Tissue Int. 2004; 75:477–481. [PubMed: 15365658]
44. Zikan V, Stepan JJ. Plasma type 1 collagen cross-linked C-telopeptide: A sensitive marker of acute effects of salmon calcitonin on bone resorption. Clin Chim Acta. 2002; 316:63–69. [PubMed: 11750275]
45. Overgaard K. Effect of intranasal salmon calcitonin therapy on bone mass and bone turnover in early postmenopausal women: A dose-response study. Calcif Tissue Int. 1994; 55:82–86. [PubMed: 7953984]
46. Tanko LB, Bagger YZ, Alexanderson P, Devogelaer JP, Reginster JY, Chick R, Olson M, Benmammar H, Mindeholm L, Azria M, Christiansen C. Safety and efficacy of a novel Eligen technology-based oral formulation of salmon calcitonin in healthy postmenopausal women: Acute and three-month effects on biomarkers of bone turnover. J Bone Miner Res. 2004; 19:1531–1538. [PubMed: 15312255]
47. Farley JR, Tarbaux NM, Hall SL, Linkhart TA, Baylink DJ. The anti-bone-resorptive agent calcitonin also acts in vitro to directly increase bone formation and bone cell proliferation. Endocrinology. 1988; 123:159–167. [PubMed: 3383771]
48. Furuichi H, Fukuyama R, Izumo N, Fujita T, Kohno T, Nakamuta H, Koida M. Bone-anabolic effect of salmon calcitonin on glucocorticoid-induced osteopenia in rats. Biol Pharm Bull. 2000; 23:946–951. [PubMed: 10963301]

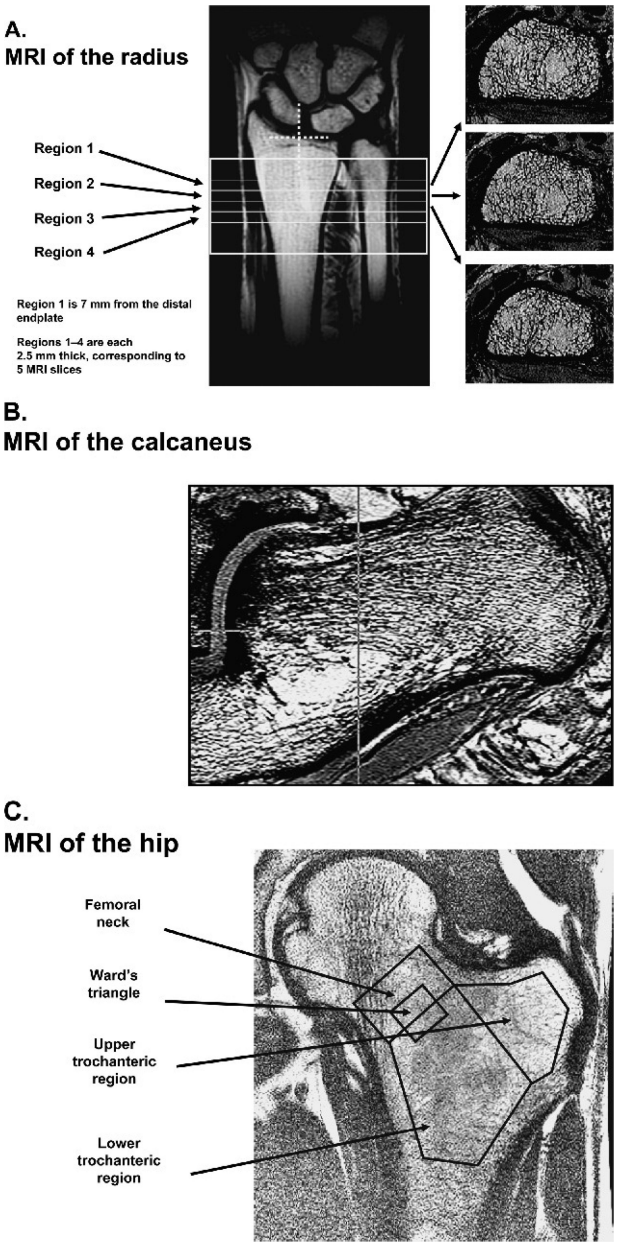

FIG. 1.

Representative MRI images at the (A) radius, (B) os calcis, (C) and hip (proximal femur), acquired using a 1.5-T General Electric Systems scanner with high resolution array coils (radius and os calcis). For the radius, four distal axial regions were assessed, three of which are shown. Region 1 is 7 mm from the distal endplate, and regions 1–4 are each 2.5 mm thick, corresponding to five MRI slices. For the hip, a coronal image with four regions of interest was obtained; for the os calcis, a sagittal image was obtained with a circular region of interest in the calcaneal area.

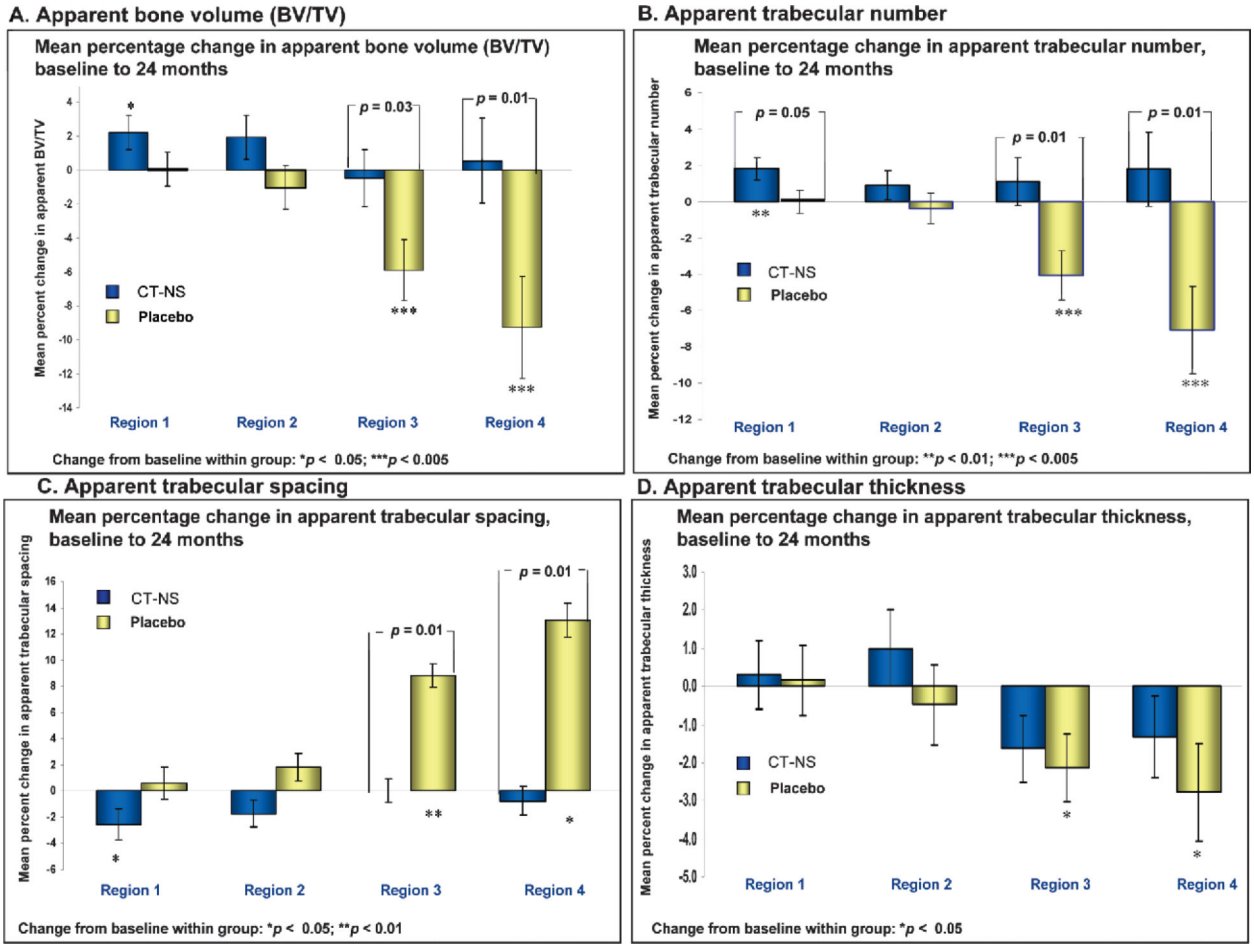

FIG. 2.

Percentage change (±SE), CT-NS versus placebo, in high-resolution MRI–acquired measurements of trabecular microarchitecture at the distal radius from baseline to 24 months: (A) apparent bone volume/total volume; (B) apparent trabecular number, (C) apparent trabecular spacing, and (D) apparent trabecular thickness. The number of subjects for each region (*n*), CT-NS: region 1, 28/26; region 2, 30/28; region 3, 31/29; region 4, 30/22 (all parameters). *Change from baseline within group; [], change from baseline between groups.

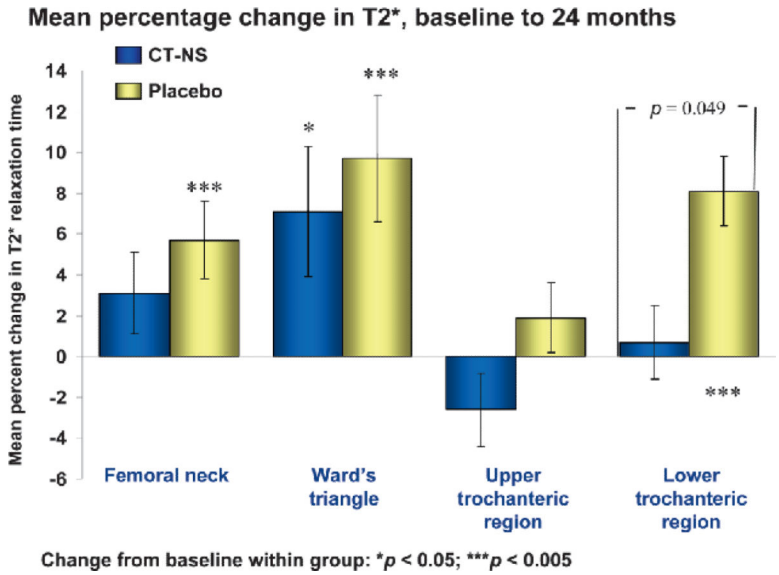

FIG. 3.

Percentage change (±SE), CT-NS versus placebo, in MRI-derived T2* relaxation times at four sites of the proximal femur, from baseline to 24 months. The number of subjects for each region (*n*), CT-NS/placebo: 30/32. *Change from baseline within group; [], change from baseline between groups.

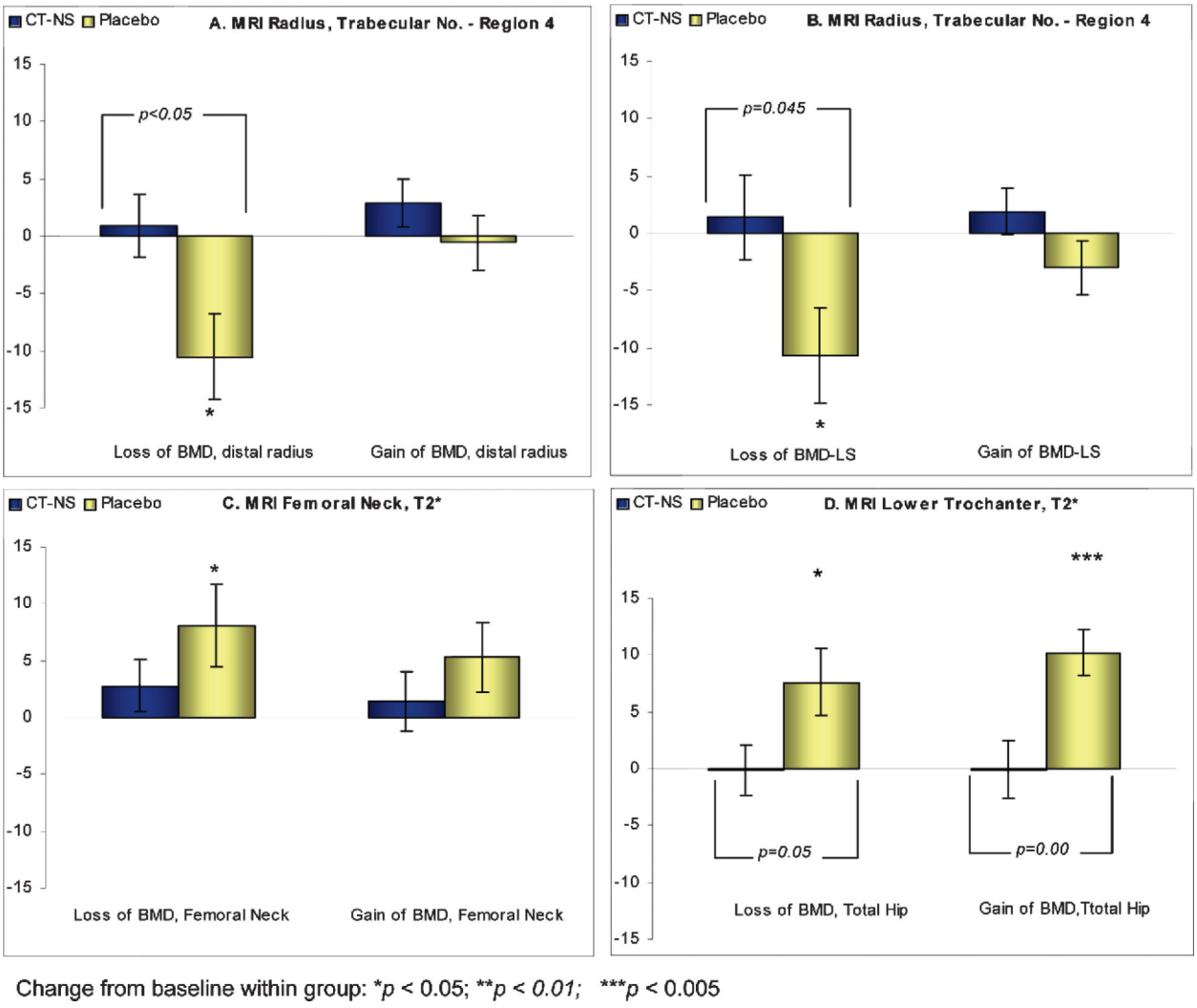

FIG. 4.

(A and B) Relationships of percent changes (±SE; gain or loss) in BMD at the distal radius or spine to percent changes in MRI microarchitecture parameters (apparent trabecular number at the radius; region 4) in CT-NS/placebo subjects from baseline to 24 months. (C and D) Relationships of percent changes (±SE; gain or loss) in BMD at the femoral neck or total hip to percent changes in MRI microarchitecture parameters (T2* at the femoral neck or lower trochanter) in CT-NS/placebo subjects from baseline to 24 months. *Change from baseline within group; [], change from baseline between groups.

Table 1

Baseline Demographic Characteristics of Enrolled Women

	CT-NS (n = 46)[*]	*Placebo (n = 45)*[*]
Age (years)	67.3 (8.0)	67.6 (8.2)
Years since menopause (years)	18.6 (9.1)	21.4 (9.8)
Number of vertebral fracture [*n* (%)]		
1	23 (50.1)	16 (35.5)
2	11 (23.9)	18 (40.0)
3	12 (26.0)	11 (24.5)
BMD of lumbar spine (g/cm^2)	0.9 (0.2)	0.8 (0.2)
Serum BSAP (U/liter)	29.0 (7.6)	28.1 (9.1)
Serum NTx (nM BCE)	13.6 (3.5)	15.0 (6.5)
Serum CTx (ng/ml)	0.5 (0.2)	0.5 (0.3)

Values are mean (SD) unless otherwise specified.

[*] Number of patients randomized to treatment arms.

Table 2

Baseline MRI Microarchitecture Parameters (Distal Radius,Hip)

	CT-NS (n = 46)[*]	*Placebo (n = 45)*[*]
Distal radius (region 4)		
Bone V./total V. app. (1/1)	0.27 (0.08)	0.29 (0.08)
Trabecular number app. (mm)	1.36 (0.28)	1.42 (0.26)
Trabecular spacing app. (mm)	0.59 (0.27)	0.55 (0.22)
Trabecular thickness app. (mm)	0.20 (0.03)	0.20 (0.03)
$T2^*$ decay time (ms) of the proximal femur		
Femoral neck	15.75 (1.89)	14.83 (2.92)
Ward's triangle	17.00 (2.69)	15.93 (4.04)
Upper trochanter	16.92 (2.01)	16.10 (2.03)
Lower trochanter	18.31 (2.12)	16.94 (2.90)

Values are mean (SD).

[*] Number of patients randomized to treatment arms.

Table 3

MRI Acquired Measurements of Trabecular Microarchitecture at Different Regions of the Distal Radius, Percentage Change From Baseline to 24 Months

	CT-NS			*Placebo*			*Treatment group comparison*		
	n	***Mean***	***Within-group p***	***n***	***Mean***	***Within-group p***	***Mean****	***95% CI***	***Between-group p***
Bone V./total V. app.									
Distal radius region 1	28	2.0	0.033	26	0.3	0.954	2.1	[–0.77;5.05]	0.145
Distal radius region 2	30	2.0	0.134	28	–1.1	0.433	3.0	[–0.69 6.64]	0.110
Distal radius region 3	31	–0.5	0.782	29	–5.9	0.002	5.4	[0.46;10.36]	0.033
Distal radius region 4	30	0.4	0.832	22	–9.1	0.003	9.8	[1.93;17.67]	0.016
Trabecular number app.									
Distal radius region 1	28	1.7	0.006	26	0.1	0.991	1.8	[0.00;3.65]	0.050
Distal radius region 2	30	0.8	0.260	28	–0.2	0.654	1.3	[–1.03;3.62]	0.270
Distal radius region 3	31	1.1	0.409	29	–4.1	0.004	5.1	[1.35;8.94]	0.009
Distal radius region 4	30	1.6	0.387	22	–6.9	0.005	8.9	[2.50;15.23]	0.007
Trabecular spacing app.									
Distal radius region 1	28	–2.3	0.032	26	0.3	0.623	–3.1	[–6.50;0.20]	0.065
Distal radius region 2	30	–1.4	0.220	28	1.5	0.210	–3.6	[–7.60;0.47]	0.082
Distal radius region 3	31	0.0	0.994	29	8.8	0.001	–8.8	[–15.49;–2.13]	0.011
Distal radius region 4	30	–0.6	0.819	22	12.9	0.001	–13.8	[–23.88;–3.76]	0.008
Trabecular thickness app.									
Distal radius region 1	28	0.3	0.745	26	0.1	0.864	0.1	[–2.47;2.73]	0.919
Distal radius region 2	30	1.2	0.324	28	–0.7	0.647	1.5	[–1.43;4.38]	0.313
Distal radius region 3	31	–1.6	0.070	29	–2.2	0.023	0.5	[–2.02;3.05]	0.688
Distal radius region 4	30	–1.3	0.228	22	–2.8	0.033	1.5	[–1.89;4.81]	0.386

*It is the least square means because the analysis was performed using an ANCOVA with baseline value as covariate.

Table 4

MRI Acquired Measurements of Trabecular Microarchitecture, Percentage Change at 2 Years, as a Function of BMD Change at Lumbar Spine

	Loss of BMD lumbar spine (n = 25)							*Gain of BMD lumbar spine (n = 27)*						
	Placebo (n = 11)			*CT-NS (n = 14)*			*Between-group p*	*Placebo (n = 11)*			*CT-NS (n = 16)*			*Between-group p*
	Mean	*SD*	*Within-group p*	*Mean*	*SD*	*Within-group p*		*Mean*	*SD*	*Within-group p*	*Mean*	*SD*	*Within-group p*	
Distal radius, region 4														
Bone V./total V. app.	–14.9	17.5	0.018	–0.5	16.2	0.901	0.045	–3.3	10.8	0.341	1.3	10.0	0.615	0.272
Trabecular number app.	–10.7	15.1	0.040	1.4	12.9	0.696	0.045	–3.0	8.4	0.260	1.9	7.6	0.335	0.126
Trabecular spacing app.	20.1	26.3	0.030	0.3	16.7	0.948	0.031	5.7	13.8	0.202	–1.4	11.9	0.638	0.165
Trabecular thickness app.	–5.1	4.8	0.006	–2.1	7.5	0.303	0.268	–0.5	4.3	0.692	–0.6	5.6	0.683	0.977
T2* decay time of the hip														
Femoral neck	9.8	14.3	0.012	–0.1	6.9	0.974	0.026	3.1	11.3	0.300	3.9	10.9	0.169	0.840
Ward's triangle	10.2	23.5	0.093	4.6	14.2	0.242	0.445	12.8	21.2	0.035	5.9	20.1	0.263	0.358
Upper trochanter	1.5	11.8	0.622	–3.2	9.0	0.211	0.240	3.7	12.6	0.268	–3.3	8.3	0.133	0.074
Lower trochanter	7.6	12.0	0.019	–0.1	8.4	0.954	0.051	10.2	8.3	0.000	–0.1	9.5	0.968	0.004

Table 5

Correlations (Standard Pearson Coefficients) Between BMD and MRI Parameters of the Forearm and Hip (Percent Change at Month 24)

BMD variable	*MRI variable*	*n*	*Correlation*	*p*
Lumbar spine	BV/TV-R1	54	0.23	0.091
	BV/TV-R2	58	–0.01	0.952
	BV/TV-R3	60	0.08	0.565
	BV/TV-R4	52	0.09	0.548
Midradius	BV/TV-R1	54	0.05	0.736
	BV/TV-R2	58	0.09	0.513
	BV/TV-R3	60	0.28	0.031
	BV/TV-R4	52	0.38	0.005
Lumbar spine	T2*-femoral neck	62	–0.11	0.410
	T2*-Ward's triangle	62	0.01	0.910
	T2*-upper trochanter	62	0.09	0.500
	T2*-lower trochanter	62	0.09	0.475
Femoral neck	T2*-femoral neck	62	–0.10	0.447
	T2*-Ward's triangle	62	0.10	0.448
	T2*-upper trochanter	62	–0.04	0.780
	T2*-lower trochanter	62	0.03	0.811

Table 6

Correlations (Standard Pearson Coefficients) Between MRI Parameters (Percent Change at Month 24) at Four Regions of the Hip (Femoral Neck,Ward's Triangle,Upper, and Lower Trochanter) vs. MRI of Four Regions of the Forearm (R1/R4)

Wrist variable	*Hip variable*	*n*	*Correlation*	*p*
BV/TV-R1	T2*-femoral neck	51	0.20	0.153
	T2*-Ward's triangle	51	0.25	0.081
	T2*-upper trochanter	51	0.21	0.131
	T2*-lower trochanter	51	0.19	0.173
BV/TV-R2	T2*-femoral neck	53	–0.02	0.911
	T2*-Ward s triangle	53	0.15	0.268
	T2*-upper trochanter	53	–0.02	0.910
	T2*-lower trochanter	53	0.01	0.997
BV/TV-R3	T2*-femoral neck	55	–0.14	0.302
	T2*-Ward s triangle	55	0.11	0.445
	T2*-upper trochanter	55	–0.18	0.185
	T2*-lower trochanter	55	–0.21	0.116
BV/TV-R4	T2*-femoral neck	46	–0.37	0.012
	T2*-Ward s triangle	46	–0.27	0.066
	T2*-upper trochanter	46	–0.35	0.017
	T2*-lower trochanter	46	–0.28	0.062